Kinase detection with gallium nitride based high electron mobility transistors

Matthew S. Makowski,[1,2] Isaac Bryan,[3] Zlatko Sitar,[3] Consuelo Arellano,[4] Jinqiao Xie,[5] Ramon Collazo,[3] and Albena Ivanisevic[3,6,a)]
[1]*Weldon School of Biomedical Engineering, Purdue University, West Lafayette, Indiana 47907, USA*
[2]*Indiana University School of Medicine, Indianapolis, Indiana 46202, USA*
[3]*Department of Materials Science and Engineering, North Carolina State University, Raleigh, North Carolina 27695, USA*
[4]*Department of Statistics, North Carolina State University, Raleigh, North Carolina 27695, USA*
[5]*HexaTech, Inc., 991 Aviation Pkwy, Suite 800, Morrisville, North Carolina 27560, USA*
[6]*Joint Department of Biomedical Engineering, North Carolina State University, University of North Carolina, Raleigh, North Carolina 27695, USA*

(Received 3 May 2013; accepted 16 June 2013; published online 1 July 2013)

A label-free kinase detection system was fabricated by the adsorption of gold nanoparticles functionalized with kinase inhibitor onto AlGaN/GaN high electron mobility transistors (HEMTs). The HEMTs were operated near threshold voltage due to the greatest sensitivity in this operational region. The Au NP/HEMT biosensor system electrically detected 1 pM SRC kinase in ionic solutions. These results are pertinent to drug development applications associated with kinase sensing. © *2013 AIP Publishing LLC*. [http://dx.doi.org/10.1063/1.4812987]

Quantification of cellular or tissue kinome activity is important in basic cell biology research[1] and drug development.[2] Label-free methods of kinome activity profiling are ideal due to elimination of artifacts caused by changes to kinase characteristics with labeling.[3] An important label-free method of kinome activity measurement is the kinase affinity assay. In this method, cell lysates are exposed to beads functionalized with small molecule kinase inhibitors that bind kinases in the cell lysate. The kinases are removed from the beads by elution, and the kinase profile is identified by mass spectrometry. The factors that affect kinome activity profiles are the amount of kinase present in the cell lysate and the kinase affinity to the inhibitor beads.[2] Affinity is in turn affected by kinase activation state as regulated by phosphorylation.[2,3]

Basic science and clinical applications exist for the kinase affinity assay. An example basic science application was the monitoring of cell cycle kinase phosphorylation status.[1] An example clinical application was a triple negative breast cancer (TNBC) drug screening study.[2] This study monitored changes in the kinome activity profile of TNBC cells with exposure to a MEK inhibitor drug. The kinome activity data guided selection of a combination of kinase inhibitor drugs in conjunction with the MEK inhibitor that resulted in decreased drug resistance compared to using any of the drugs alone.[2] Monitoring of the entire kinome gave a better overall view of drug efficacy than by monitoring the activity of a single kinase where drug resistance often develops by compensatory upregulation of uninhibited kinases.[2] Another clinical application of the kinase affinity assay was in drug development through determining kinase inhibitor drug targets.[3] Cell lysates were treated with soluble kinase inhibitors, and the lysates were exposed to the affinity beads. The soluble drug bound its target kinases, and the remaining kinases had their ATP binding sites available to bind the beads of the affinity assay.[3] The kinases with a decreased representation based on mass spectrometry following drug treatment were identified as the drug targets.[3]

In this proof-of-concept report, we have demonstrated label-free detection of a kinase by a nanoparticle (NP)/high electron mobility transistor (HEMT) biosensor system. This detection method excluded the complication of a sequential kinase affinity assay followed by mass spectrometry analysis. Gold (Au) NPs were functionalized with PP58 to serve as a receptor to trap SRC kinase for electrical detection by AlGaN/GaN HEMTs. PP58 is one of the pyrido[2,3-d]pyrimidines which are small molecule broad kinase inhibitors that inhibit SRC kinase among other tyrosine and serine/threonine kinases by competitive inhibition at the ATP binding site.[4] PP58 was used because it retains its activity when attached to solid substrates and it has a wide range of target kinases.[2,4] SRC kinase was chosen as a model analyte since the literature shows that it binds to PP58 on beads,[4] it is an important cytoplasmic tyrosine kinase involved in regulation of cellular functions such as proliferation and differentiation,[5] and it is implicated in some breast and colon cancers.[6] In the work presented here, buffer solutions were spiked with various concentrations of SRC kinase, and the changes of transistor electrical characteristics were measured following exposure to the SRC solutions.

The gold nanoparticle conjugation kit was purchased from Ocean Nanotech, LLC and included 30 nm carboxyl terminated gold nanoparticles, N-ethyl-N′-dimethylaminopropyl-carbodiimide (EDAC), gold reaction buffer, and wash/storage buffer. N,N-dimethylformamide (DMF), ethanolamine, and bovine serum albumin (BSA) were purchased from Sigma-Aldrich. Ethanol was purchased from Pharmco-Aaper. Kinase buffer A (KBA, contains 250 mM HEPES (pH 7.5), 50 mM $MgCl_2$, 5 mM EGTA, and 0.05% Brij-35), and SRC kinase was purchased from Life Technologies Corporation.

The AlGaN/GaN HEMTs, Figure 1(a), were fabricated as reported earlier.[7] The kinase inhibitor PP58 was conjugated to Au NPs to serve as a receptor for SRC kinase. The conjugation protocol proceeded by activating the Au NPs

a)Author to whom correspondence should be addressed. Electronic mail: ivanisevic@ncsu.edu

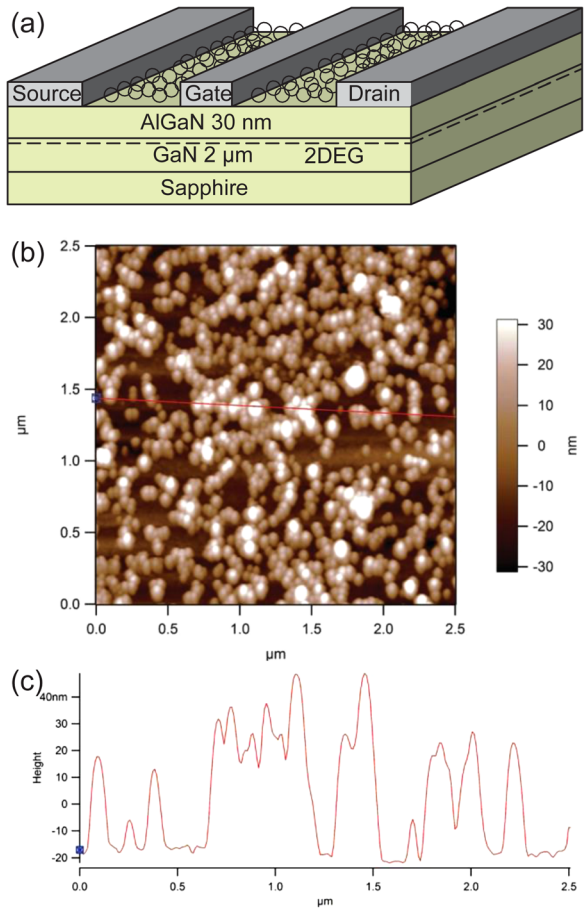

FIG. 1. (a) Diagram of the HEMT structure used in this work. The adsorption of nanoparticles was not limited to the transistor channels as shown here. The diagram is not drawn to scale. (b) Representative AFM image of PP58-NPs physisorbed above the channel of a transistor. (c) Cross-section of the AFM image in (b).

with EDAC and forming an amide bond with the terminal amine group of PP58. This procedure was demonstrated in the literature with Sepharose beads,[2] and further protocol details are included in the supplementary material.[8] To physisorb the Au NPs on the transistor surfaces, 5 to 10 μl of the PP58-NP solution was spotted onto each 3 mm × 3 mm wafer and dried in a vacuum desiccator. The wafers were submerged in KBA several times to remove loosely adhered NPs and dried with nitrogen gas. Figures 1(b) and 1(c) display a representative AFM image and cross-section of PP58-NPs physisorbed to the channel area of a transistor.

Four wafers were processed in this experiment. Two wafers were the treatment wafers and the other two were the control wafers. The first treatment wafer consisted of 8 transistors that were sequentially treated by a 60 min exposure to KBA, increasing concentrations of SRC in KBA, and 610 μM BSA in KBA. The second treatment wafer consisted of 8 transistors that were sequentially treated by a 15 min exposure to KBA and 3 min exposures to increasing concentrations of SRC in KBA. The KBA exposures tested for the effects of the salts in the buffer on transistor electrical properties. The increasing SRC concentrations ranged from 1 fM to 100 nM. These concentrations were used to determine where the transistor output saturated. The exposure to BSA tested the specificity of the sensor when the receptors were occupied with SRC. The first control wafer consisted of 6 transistors that were sequentially treated by 60 min exposures to KBA five times and 610 μM BSA in KBA. The second control wafer consisted of 8 transistors that were sequentially treated by a 240 min exposure to KBA and a 3 min exposure to 610 μM BSA in KBA. The experiments with the control wafers tested the effects of KBA on transistor output and the specificity of the sensor to BSA when the receptors were unoccupied with SRC. Figure 2 diagrams the sequential treatments of the treatment and control wafers.

For each treatment, the wafers were placed in wells of a 96 well plate and 50 μl of KBA, SRC solution, or BSA solution was added to each well depending on which treatment was applied. The wafers were incubated in solutions for 3, 15, 60, or 240 min at room temperature. Unbound protein was washed from the wafer surfaces by discarding well contents, adding 200 μl KBA, and agitating gently for 3 min. This washing procedure was repeated a total of four times. After washing, the wafers were dried with nitrogen gas.

Drain current (I_D) was measured for each transistor in its initial state and following each treatment including PP58-NP spotting and exposures to KBA, SRC, and BSA. Two different drain to source voltage (V_{DS}) and gate to source voltage (V_{GS}) configurations were used. The first configuration was used to estimate the threshold voltage (V_t). This configuration swept V_{GS} from 0 to −3 V by −0.005 V increments with $V_{DS} = 0.5$ V. The second configuration was used to calculate relative ΔI_D at the optimal operating point following each treatment. This configuration swept V_{DS} from 0 to 4 V by 0.05 V increments, and V_{GS} was stepped from 0 to −3 V by −0.25 V steps.

The optimal operating point was calculated for each transistor before any treatments were applied. As demonstrated previously, the optimal operating point was where the drain and gate biases (V_{DS} and V_{GS}) maximized $(dI_D/dV_{GS})/I_D$ such that a change in V_{GS} gave the greatest relative change in I_D.[7] For the transistors tested in this study, the optimal operating points were at $V_{DS} = 0.05$ to 0.5 V and $V_{GS} = -1.75$ to −2.25 V. The relative ΔI_D values reported in

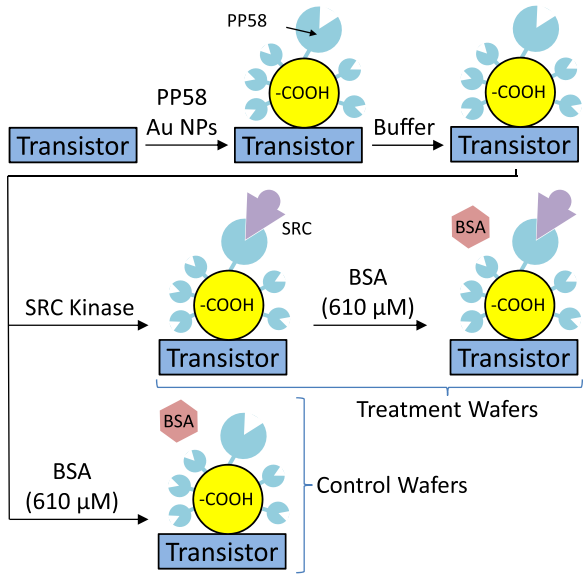

FIG. 2. Representation of the treatments applied to transistors of the treatment and control wafers.

Figures 3 and 4 were calculated as relative $\Delta I_D = (I_{Dt} - I_{Di})/I_{Di}$, where I_{Dt} is the drain current at the optimal operating point following the respective treatment and I_{Di} is the drain current at the optimal operating point before any treatments were applied. V_t was estimated by the linear extrapolation method from the I_D versus V_{GS} curve by finding where an extrapolated line at the greatest slope intersected the V_{GS} axis.[9] ΔV_t values reported in Figures 3 and 4 were calculated as $\Delta V_t = V_{tt} - V_{ti}$, where V_{tt} is the threshold voltage following the respective treatment and V_{ti} is the initial threshold voltage of the transistor before any treatments were applied.

A separate ANOVA was conducted on the relative ΔI_D and ΔV_t values for the transistor sample sets on each of the treatment and control wafers. Transistors within a sample set were modeled as blocking factors to control for transistor-to-transistor variation. Comparisons between means of relative ΔI_D or ΔV_t were conducted by calculating the critical difference between means with Tukey's Method at $p < 0.05$.[10]

To test the operation of the transistor biosensors, the transistors on each treatment wafer were exposed to increasing concentrations of SRC solutions. These transistors were also exposed to a neat buffer solution (KBA), and the transistors on the first treatment wafer were also exposed to a solution of BSA. BSA was chosen due to its size and isoelectric point (pI) similarities to SRC. The molecular weights of

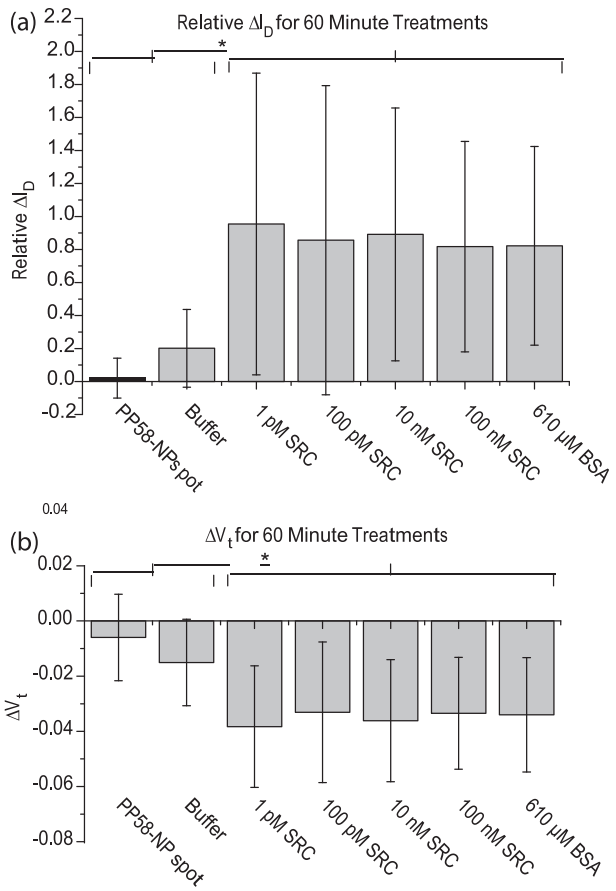

FIG. 3. Relative ΔI_D (a) and ΔV_t (b) following each treatment for the transistors on the first treatment wafer. Buffer (KBA), SRC in KBA, and BSA in KBA exposure durations were 60 min. Means and standard deviations are shown. The asterisks indicate significant difference at $p < 0.05$ using ANOVA and comparing means with Tukey's method. The mean and standard deviation of initial V_t are -1.85 ± 0.03 V.

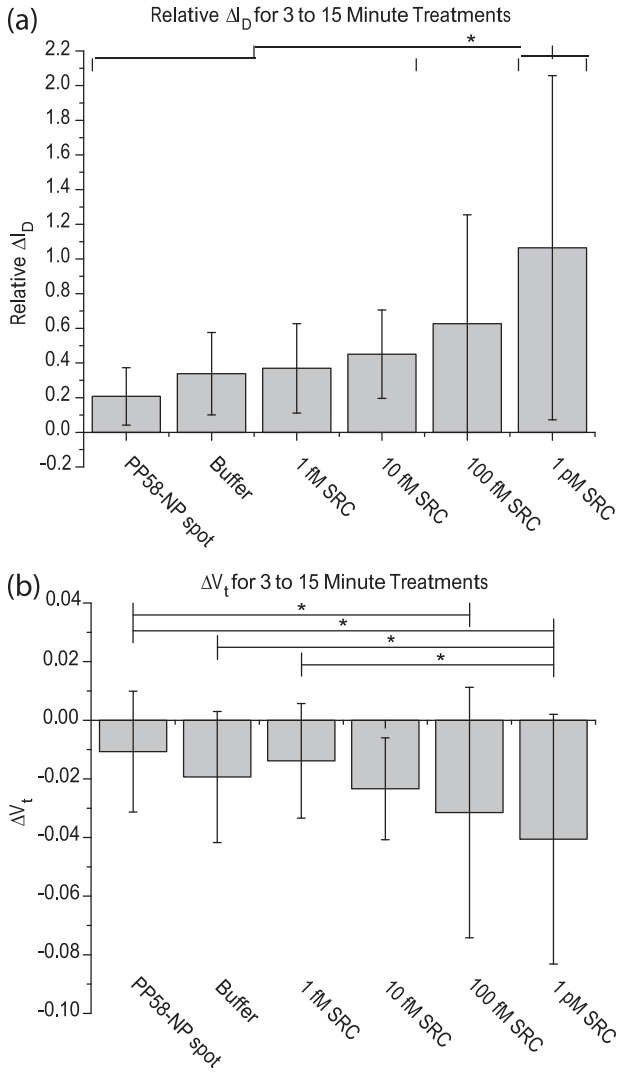

FIG. 4. Relative ΔI_D (a) and ΔV_t (b) following each treatment for the transistors on the second treatment wafer. Buffer (KBA) exposure duration was 15 min. SRC in KBA exposure durations were 3 min. Means and standard deviations are shown. The asterisks indicate significant difference at $p < 0.05$ using ANOVA and comparing means with Tukey's method. The mean and standard deviation of initial V_t are -1.81 ± 0.02 V.

SRC and BSA are 62.3 kDa and about 66 kDa, respectively. Using SRC in murine fibroblasts as a comparison, the pI of SRC is 4.35 to 5.05.[5] The pI of BSA is 4.7 to 4.9.[11] The BSA concentration of 610 μM corresponds to a clinically relevant level of albumin in human adult serum at 35–55 g/l (530–833 μM).[12]

Figure 3(a) shows the relative ΔI_D of the transistors on the first treatment wafer following deposition of PP58-NPs and 60 min exposures to KBA, increasing concentrations of SRC in KBA, and 610 μM BSA in KBA. The deposition of PP58-NPs caused a negligible relative ΔI_D. Following exposure to KBA, the transistors had a small increase in relative ΔI_D that was likely caused by nonspecific deposition of salts in the buffer. Additional washing steps may improve upon this nonspecific salt adsorption. The most important result is the significant increase in relative ΔI_D when the transistors were exposed to 1 pM SRC kinase for 1 h. This indicates that SRC bound the PP58-NPs near the transistor surfaces, and the electrical charge on the SRC increased transistor conductance. Since AlGaN/GaN HEMTs are n-type channel

field-effect devices, the increase in relative ΔI_D indicates binding of a positively charged analyte at the transistor surfaces.[13] With each additional SRC treatment of increasing concentration, it was expected that the transistor responses would increase. However, the transistor responses seem to have saturated since relative ΔI_D values following the remaining treatments were not significantly different. One explanation is that the PP58 molecules on the NPs were all occupied with a SRC molecule following the initial SRC treatment. This may have resulted from the long duration (1 h) of SRC exposure, a low PP58 coverage of the NPs, or a low surface density of PP58-NPs on the transistors. Finally, the exposure of the transistors to 610 μM BSA did not cause a significant relative ΔI_D change. Since the PP58 receptors were likely already occupied by SRC, the lack of response to BSA indicates that nonspecific adsorption of BSA on the transistor surfaces did not happen to an extent great enough to affect transistor responses.

The mechanism of I_D change by analyte binding near the gate surface of a field-effect transistor is by a shift in V_t.[14] Figure 3(b) shows the shifts in V_t relative to initial state with each treatment for the transistors on the first treatment wafer. As expected, the statistical analysis matches that of Figure 3(a) with a significant difference between the group of treatments before and after exposure to SRC kinase. Since AlGaN/GaN HEMTs are n-type channel field-effect devices, the negative ΔV_t also supports the presence of a positively charged species at the transistor surfaces.[15]

The first control wafer with a set of six transistors was spotted with PP58-NPs, exposed to buffer (KBA) for five separate 1 h durations, and exposed to 610 μM BSA for 1 h. The second control wafer with eight transistors was spotted with PP58-NPs, exposed to KBA for 4 h, and exposed to 610 μM BSA for 3 min. A separate ANOVA was conducted on the set of transistors of each control wafer, and mean comparisons with Tukey's method resulted in no significant differences among the ΔI_D values following each treatment at $p < 0.05$ (data not shown). These results indicate that buffer and BSA exposure did not produce significant transistor biosensor responses.

As shown in Figure 3(a), the response of the transistors on the first treatment wafer saturated at the lowest SRC concentration tested (1 pM). To test the dynamic range of the PP58-Au NP/HEMT biosensor, the transistors on the second treatment wafer were exposed to lower SRC concentrations for shorter durations. After depositing the PP58-NPs, the transistors were exposed to buffer (KBA) for 15 min followed by 3 min exposures to increasing SRC concentrations (1 fM to 1 pM). Figure 4(a) displays the statistically significant increase in relative ΔI_D when the transistors were exposed to 1 pM SRC compared to KBA, 1 fM SRC, and 10 fM SRC. Figure 4(b) shows a statistically significant ΔV_t when the transistors were exposed to 1 pM SRC compared to KBA and 1 fM SRC. These results indicate that for a sample size of 8 transistors, 1 pM of SRC is detectable in an ionic solution after only 3 min of exposure. Figure 4(a) also shows a linear increase in mean transistor response when SRC kinase concentration was raised in tenfold increments.

For now, the primary disadvantage of the NP spotting method is the variability of NP surface density across wafer surfaces. The statistical analysis method used does not account for interaction effects between transistors and treatments. This interaction is likely to arise with variability in PP58-NP density from transistor-to-transistor. Transistors with a greater density of NPs will likely have a greater density of surface receptors and thus a greater response to a given SRC kinase concentration. A more complex statistical model that accounts for this interaction effect may provide additional insight. The other disadvantage of the NP spotting method is that the device is not yet optimized for real-time analyte detection since electrical measurements require drying the wafer following each treatment. In future studies, the incorporation of the transistor sensors into microfluidic systems can offer a user-friendly platform for controlled delivery of samples to the sensor transducer.

In summary, the PP58-Au NP/HEMT biosensor detected SRC kinase at a concentration as low as 1 pM in an ionic solution. Also, the sensor had a relatively low response to neat buffer and a clinically relevant concentration of nonspecific protein. These results indicate that the system of functionalized Au NPs physisorbed to AlGaN/GaN HEMTs provides a promising route of kinase detection with potential applications in drug development and basic cellular biology research.

This work was supported by NSF under CMMI-0856391, NIH/NCRR-Indiana Clinical and Translational Sciences Institute–TL1 Program under TL1 RR025759 (A. Shekhar, PI), and the Indiana University Medical Scientist Training Program under NIH GM077229. We thank Professor Charles Proctor (Department of Statistics, NCSU) for advice on statistical analysis and Professor Gary Johnson (Department of Pharmacology, UNC-Chapel Hill) for helpful discussions and a generous donation of PP58.

[1]H. Daub, J. V. Olsen, M. Bairlein, F. Gnad, F. S. Oppermann, R. Körner, Z. Greff, G. Kéri, O. Stemmann, and M. Mann, Mol. Cell **31**(3), 438 (2008).
[2]J. S. Duncan, M. C. Whittle, K. Nakamura, A. N. Abell, A. A. Midland, J. S. Zawistowski, N. L. Johnson, D. A. Granger, N. V. Jordan, D. B. Darr, J. Usary, P. F. Kuan, D. M. Smalley, B. Major, X. P. He, K. A. Hoadley, B. Zhou, N. E. Sharpless, C. M. Perou, W. Y. Kim, S. M. Gomez, X. Chen, J. Jin, S. V. Frye, H. S. Earp, L. M. Graves, and G. L. Johnson, Cell **149**(2), 307 (2012).
[3]M. Bantscheff, D. Eberhard, Y. Abraham, S. Bastuck, M. Boesche, S. Hobson, T. Mathieson, J. Perrin, M. Raida, C. Rau, V. Reader, G. Sweetman, A. Bauer, T. Bouwmeester, C. Hopf, U. Kruse, G. Neubauer, N. Ramsden, J. Rick, B. Kuster, and G. Drewes, Nat. Biotechnol. **25**(9), 1035 (2007).
[4]J. Wissing, K. Godl, D. Brehmer, S. Blencke, M. Weber, P. Habenberger, M. Stein-Gerlach, A. Missio, M. Cotten, S. Müller, and H. Daub, Mol. Cell Proteomics **3**(12), 1181 (2004).
[5]R. Palumbo, F. De Marchis, T. Pusterla, A. Conti, M. Alessio, and M. E. Bianchi, J. Leukoc. Biol. **86**(3), 617 (2009).
[6]G. S. Martin, Nat. Rev. Mol. Cell Biol. **2**(6), 467 (2001).
[7]M. S. Makowski, S. Kim, M. Gaillard, D. Janes, M. J. Manfra, I. Bryan, Z. Sitar, C. Arellano, J. Xie, R. Collazo, and A. Ivanisevic, Appl. Phys. Lett. **102**(7), 074102 (2013).
[8]See supplementary material at http://dx.doi.org/10.1063/1.4812987 for further details of the Au NP/PP58 conjugation protocol.
[9]A. Ortiz-Conde, E. G. Fernandes, J. J. Liou, M. R. Hassan, F. J. G. Sanchez, G. DeMercato, W. Wong, and O. M. Castillo, in *Proceedings of the 21st International Conference on Microelectronics* (1997), Vol. 1, p. 285.
[10]D. C. Montgomery, *Design and Analysis of Experiments*, 7th ed. (John Wiley & Sons, Inc., 2009).

[11]F. Kratz, C. Müller, N. Körber, N. Umanskaya, M. Hannig, and C. Ziegler, Phys. Status Solidi A **210**, 964–967 (2013).
[12]D. L. Kasper, E. Braunwald, A. S. Fauci, S. L. Hauser, D. L. Longo, and J. L. Jameson, *Harrison's Principles of Internal Medicine*, 16th ed. (McGraw-Hill Companies, Inc., 2005).
[13]S. Gupta, M. Elias, X. J. Wen, J. Shapiro, L. Brillson, W. Lu, and S. C. Lee, Biosens. Bioelectron. **24**(4), 505 (2008).
[14]P. Bergveld, Sens. Actuators, B **88**(1), 1 (2003).
[15]R. F. Pierret, *Semiconductor Device Fundamentals* (Addison-Wesley Publishing Company, 1996), p. 675.